

Effect of Plasmonic Coupling in Different Assembly of Gold Nanorods

Aditya K. Sahu and Satyabrata Raj*

Department of Physical Sciences, Indian Institute of Science Education and Research Kolkata

Mohanpur, Nadia, 741246, India

Abstract

The influence of the orientation of gold nanorods in different assemblies has been investigated using the Finite Difference Time Domain (FDTD) simulation method. To understand the relative orientation, we vary the size and angle in dimer geometries. Significant effects of plasmon coupling emerged in longitudinal resonances having end-to-end configurations of gold nanorods. The effect of orientational plasmon coupling in dimers gives rise to both bonding and anti-bonding plasmon modes. Effects of various geometries like primary monomer, dimer, trimer, and tetramer structures have been explored and compared with their higher nanorod ensembles. The asymmetric spectral response in a 4×4 gold nanorods array indicates a Fano-like resonance. The variation of gap distance in ordered arrays allowed modulation of the Fano resonance mode. The resonance wavelength and field enhancement of the plasmon modes have been tuned by varying the gap distance, angular orientation, size irregularity between the nanorods, and nanorod numbers in an array. The integrated nanostructures studied here are not only significant for fundamental research but also applications in plasmon-based devices.

1. Introduction

Metallic plasmonic nanostructures have received significant interest for even more than a decade due to their use in enhancement and imaging applications,¹⁻⁴ non-linear and quantum optics,⁵⁻⁸ ultra-fast switches,⁹ and photovoltaic systems.^{10,11} In metallic plasmonic material research, gold nanostructure occupies a prominent place, and their extensive optical properties have been illustrated in several studies. Therefore, various works have been done to develop and produce multiple metallic nanostructures to satisfy various application requirements. For all the applications, substantial field enhancement and tuning of surface plasmon resonance are mainly required. It is noteworthy to mention that the most exciting feature of the gold nanorods (GNRs) is their longitudinal surface plasmon resonance (LSPR).¹² The intensity, frequency, and consistency of the LSPR in an individual GNR is sensitively dependent on the dimension like size and geometry and the surrounding environment (refractive index) along with the presence of other gold nanoparticles nearby.^{13,14} Plasmonic structures containing dimers, trimers, and various array geometries have recently received much interest, as they give a tunability of optical properties of the system. The electromagnetic field and the wavelength can be substantially tuned by the separation gap and geometry orientation of the individual components in the plasmonic structure.¹⁵⁻¹⁷ This remarkable ability allows maximum electrical field enhancements around the nanorods by providing a spectrum of light-matter interactions with new mechanisms.

In general, the chemical synthesis method produces a cluster of nanoparticles with much smaller separations with a proper plasmonic response, but the particles inside the cluster can have a wide distribution of different shapes and sizes.¹⁸ Consequently, the assembly of nanoparticles would inevitably involve local irregularities in neighboring particle's geometry and spacing. The LSPR of the combined cluster, particularly in overlapping particles, will be affected

in the assembly, enhancing the excitation of charge transfer plasmons.^{19,20} The several new phenomena in dimers and larger structures composed of anisotropic particles make the relative orientation between nanorods an important parameter.

The surface plasmon coupling is considered to be the hybridization of different surface plasmon resonance modes^{21,22} and the synthesis of ideal dimers in a laboratory is quite difficult. The relative orientation of the nanoparticles in non-ideal dimers produces different gaps in surface morphology. The plasmon coupling induced by the assembly of organized gold nanorods leads to substantial electric field enhancements along with different collective plasmon responses.²² The study of the optical properties of these structures will help to understand how light is interacting with the matter, and as a consequence, plasmon couplings between metal nanorods can be used to enhance Raman signals, second-harmonics, fluorescence, photoluminescence, and nanometric optical tweezers.²³⁻²⁷ Metallic nanorods with a close gap can act as optical nano-antennas due to the plasmon coupling-induced large electric field enhancement.^{28,29}

In general, surface plasmon absorption bands evolve from the oscillations of conduction electrons in transverse and longitudinal directions. The overall spectra do not give much information about transverse oscillations and based on its longitudinal surface plasmon resonance, the correlation of a single nanorod into a more extensive assembly is typically studied. Hybridization of plasmon modes can be in-phase or out-of-phase when two metal nanorods interact between themselves. Depending upon the polarization of source light, bonding and anti-bonding modes arise. It has been found that the in-phase hybridization mode, i.e., bonding mode, which is red-shifted in LSPR frequency and strengthens the electric field at the junction of nanorods, arises when the polarized source light is along the nanorod axis. The out-

of-phase hybridization mode, i.e., anti-bonding mode, contributes to the blue-shifted LSPR frequency and appears at the non-junction end of the nanorods.^{14,30} However, the LSPR change and plasmon coupling for transverse polarization where the polarization of light is perpendicular to the nanorod axis is minimal.¹⁴ In the ordered array of nanoparticles, the presence of red-shifted narrow peaks is due to the coupling of localized plasmon resonance of individual particles and the collective photonic modes of the ordered array ensembles and can be interpreted as a Fano-like interference model.³¹ The interactions between the bonding and antibonding modes of the plasmonic system lead to Fano resonances. In certain instances, coupling effects can generate Fano-like resonances in plasmonic structures. The impact of plasmonic Fano resonances has lots of applications in meta-materials, signal enhancement, and sensors, etc.^{32,33} Many simulation studies demonstrate that one can tune the Fano resonance of a structure by varying the incident light polarization³² and refractive index of the surrounding medium,³⁴ which makes it a good candidate for potential application in chemical sensors.³³ In spite of a lot of studies on Fano resonance in various systems, we have little knowledge on how the morphological change and the separation distances between the nanoparticles in the ordered array are affected by the coupling strength of different plasmonic modes.

In a few recent studies, the significance of the nanorod orientation on the plasmon coupling has been pointed out; however, the effect on the plasmon coupling of the angle between nanorods in dimers is not yet fully explored. We have investigated the irregularities in coupled LSPRs of nanorod dimers and many different structures using the finite difference time domain (FDTD) simulation method. The theoretical calculations for gold nanorod dimers were carried out on different orientations such as end-to-end, side-by-side, and various array positions to observe their effect with these parameters. In a nanorod assembly, the angular degrees of

freedom complicate the prediction of LSPR interactions. Our present studies have simulated the plasmon coupling in Au nanorod dimers by changing the relative angle between two nanorods. We found bonding and antibonding modes due to plasmon hybridization of individual nanorod when one nanorod is rotated with respect to another one in a dimer (with same size nanorods and gap of 3 nm separation). Size mismatch of nanorods in dimers also has a tremendous effect on the optical properties, which is also studied here. A thorough understanding of the effect of size mismatch on the collective optical properties of nanorod dimers has been reviewed here. Theoretically, we also describe a structural geometry of gold nanorods of 4×4 matrices, illuminated under normal incidence, presenting a fano-resonance when separated by a finite gap. The near field aspects, particularly electric field enhancements, have been explored and interpreted with the existing results. We address mainly the plasmon coupling with reliance on four variables: separation, orientation, size heterogeneity, and the number of nanorods in an array of geometry. Correlating the intensities and LSPRs positions in these structural variations of gold nanorod geometries is vital to understand the effect of irregularities in geometry on plasmon coupling, which is a true scenario in real chemically grown geometry nanorods. To optimize the design and applications of near-field, understanding the plasmon coupling is very much required and is of prime interest.

2. Simulation Methodology

Electromagnetic simulations have been carried out to understand the surface plasmonic properties in various nanorod assemblies by using the FDTD simulation method. FDTD simulation is one of the most common computing tools for numerically solving Maxwell electromagnetic time-dependent equations and the same has been used to model our nanostructures optically.³⁵ Drude dielectric function has been used along with the experimental

results to model metallic gold nanorods. We have used a mesh of 0.5 nm in our simulation for the convergence criteria. We used perfectly matched layer (PML) boundary conditions to prevent any non-physical scattering at boundaries. We used the experimental results of Johnson and Christy to model the complex permittivity of gold.³⁶ We used the Total Field Scattered Field (TFSF) as the source. We used a power monitor, one for the computation of the absorption coefficients inside the TFSF source and another for the scattering coefficients outside the source. The polarization of incident light has been set along the nanorods to analyze the longitudinal plasmonic response of the different geometries.

3. Results and Discussions

The plasmonic coupling has been studied by changing the nanorod size and the alignment of nanorods (rotational geometries) to each other in the dimer configuration. The study has been carried out to understand and model the coupling between anisotropic nanorods, especially when the aspect ratio of one nanorod increases by keeping the aspect ratio of another nanorod constant and understanding the effect when nanorods are rotating with each other in the dimer. The longitudinal antibonding mode would not be illuminated for linear homo-dimers, as antiparallel dipoles do not create a net dipole for the dimer.²⁰ We studied the effects of various factors breaking the structure's homogeneity to explain why antibonding modes appear in the spectrum. The two significant sources of inhomogeneity in dimers are the angular orientation of nanorods [Figure 1(a)] and the irregularity of size between the two nanorods [Figure 1(b)].

We have analyzed the role of the relative orientation of nanorods in dimers on plasmon coupling. To understand the linear geometry deviation in homo-dimers, we have considered nanorods of equal dimensions (70×30 nm) with $AR = 2.33$ and having a separation of 3 nm

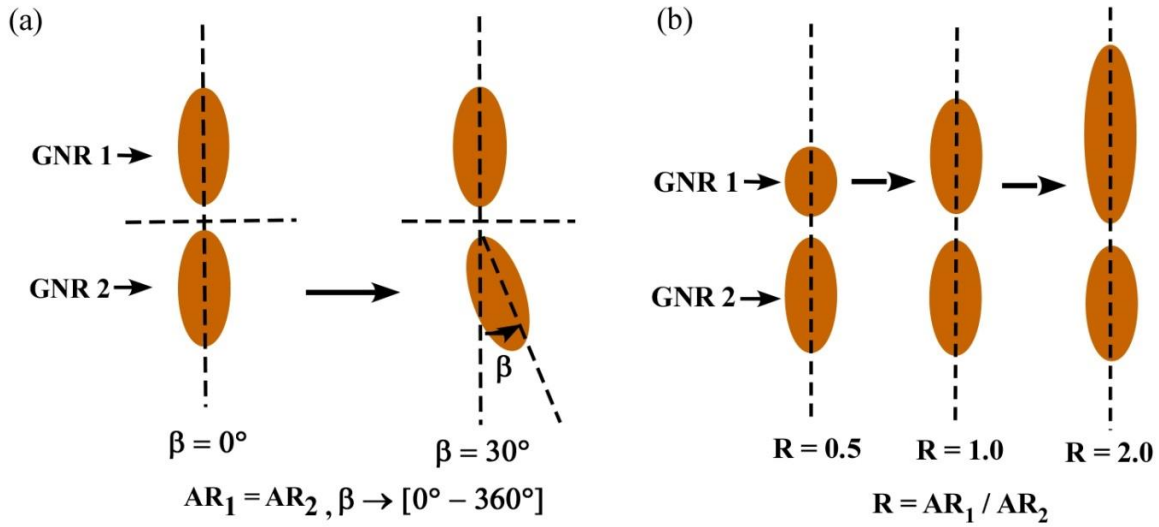


Figure 1. The schematic orientation of nanorods in the dimer (a) with angular rotation, β keeping ratio, $R = 1.0$ (b) with two different size nanorods in end-to-end coupling.

with an offset angle, β between them. We observed the absorption spectra of dimers in figure 2, where light polarization is aligned along the nanorod axis, and one nanorod placed relative to another nanorod at different angular orientations. Bonding and antibonding peaks that arise with angular variation are demonstrated in Figures 2(a) and 2(b). As nanorods come very close, i.e., conductive contact, new spectral features for the dimers are evolved, which change the optical properties of dimers. Such conductive contact facilitates plasmon modes which involve the polarization of the charge distribution all over the nanorods and the electric field oscillation between the junctions of nanorods. When a nanorod rotates w.r.t another one by keeping the polarization of the incident light along the nanorod axis, the hybridized plasmon dipole along the nanorod axis becomes blue-shifted due to reduced coupling between nanorods in a dimer. The decoupling of the plasmonic modes happens due to the decrease in the tip-to-tip coupling between the nanorod surfaces as one rod rotates around its center of mass.³⁷

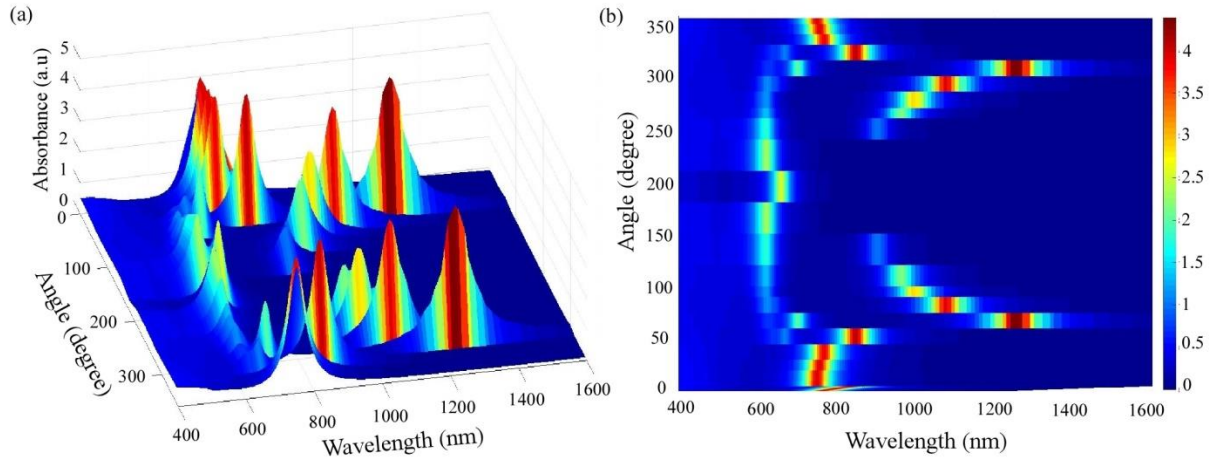


Figure 2. (a) Plasmon coupling vs. angle, β between nanorods in dimer and (b) variation of LSPR peak position w.r.t angular offset, β (top view).

To understand a deep insight into dimers' plasmonic properties, a simple plasmonic hybridization picture is adopted to explain its electromagnetic behavior. The dimers in-plane plasmon modes have been considered in our FDTD calculations with the polarization of light is either parallel or perpendicular to the bisector of angular offset, β inside the substrate plane. In this assumption, four hybridized plasmon modes are expected due to individual transverse and longitudinal plasmon modes of each nanorod in the dimer.¹⁷ Both modes hybridize separately in alignment with the orientations of end-to-end and side-by-side to provide a bonding and anti-bonding mode when the angle between the nanorods becomes 0° and 180° , respectively. The FDTD calculation shows that the transverse anti-bonding and longitudinal bonding modes are active at 0° , whereas the transverse mode is indistinguishable and showing a single peak around 752 nm. The absorption peaks from the longitudinal anti-bonding and transverse bonding modes are active at 180° , but one single peak at 662 nm appears due to longitudinal polarization. As the size/geometry of the nanorod dimer reduced, these two modes cannot be described anymore by the combination of individual nanorod modes. Instead, it provides new plasmon modes, which

are classified as bonding and anti-bonding modes. Due to the geometry irregularities, the transverse and longitudinal modes are mixed. The observed electric field distributions indicate that the longitudinal dipolar modes of each nanorod ultimately contribute to the hybridized modes.³⁸ The most exciting feature of bonding and anti-bonding modes of dimers appears in the gap region. With the variation in angular offset, β , as shown in Figure 3, we have discussed the corresponding variation in LSPR and maximum enhancement in electric fields. It has been found that the electrical field of the gap region is greatly enhanced and reduced when nanorods are resonantly excited about their bonding and anti-bonding modes, respectively.

Figure 3 illustrates the symmetry pattern in the properties between the intervals 0° - 180° and 180° - 360° . As a result, we can relate the properties observed in the 0° - 180° span to those observed in the 180° - 360° . We observed a single absorption peak in the spectrum for the angle, β in the ranges $0^\circ < \beta < 45^\circ$ and $150^\circ < \beta < 180^\circ$ whereas, two absorption peaks have been observed when the angle varies in between $\sim 45^\circ$ and $\sim 150^\circ$. Also, as the angle β increases from 60° , the strength of the bonding mode decreases, whereas the intensity of the anti-bonding mode increases, which is observed around 625 nm. The bonding mode features are more sensitive as compared to the anti-bonding peak to the angular orientation, β . Only bonding peak is formed for $\beta < 45^\circ$, whereas, anti-bonding peak exists for $\beta \geq 45^\circ$ in the spectrum. The presence of anti-bonding mode arises from the coupling of the near field of the nanorods and/or the net non-zero dipole moment arising from the tilted dimer structure.³⁹ The anti-bonding plasmonic mode is characterized by a change in charge that shifts away from the center of the gap of nanorods in dimer configurations. We can correlate the enhancement of the electric field to the bonding mode

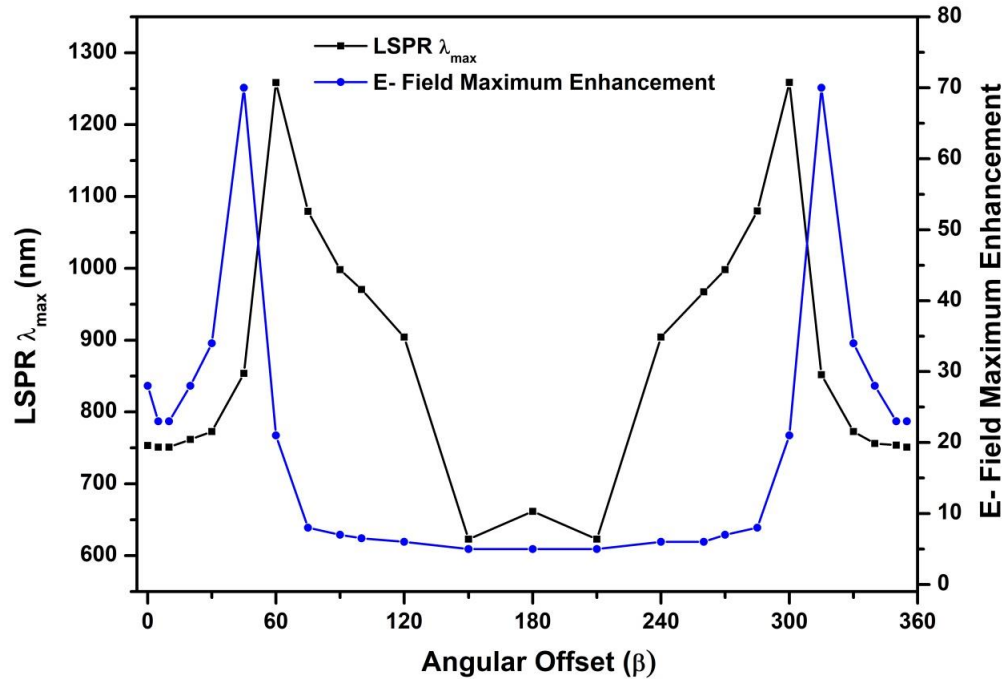


Figure 3. Variation of Longitudinal resonance and electric field maximum enhancement w.r.t. angular offset, β .

peak position and intensity. We see an improvement in field strength as the intensity of bonding mode approaches towards angular offset 60° . The intensity of bonding mode decreases after 60° , resulting in reduced field enhancement, and later nearly the same field enhancement in the 120° - 240° range, where the antibonding mode is the dominant peak. As the bonding mode dominates again, the rise in electric field intensity displays a maximum increase of around 300° . The electric field enhancement is most significant around 60° and 300° , which is also the highest bonding mode peak angle. The tilted dimer spectrum from $0^\circ < \beta < 360^\circ$ clearly shows the different bonding and anti-bonding mode contributions to absorption wavelength, intensity, and electric field enhancement. This symmetry trend between the absorption properties and the angle,

β described above could form the basis of nanoscale devices. Devices may be designed to calculate the tilted angles for dimers composed of similar sizes of nanorods.

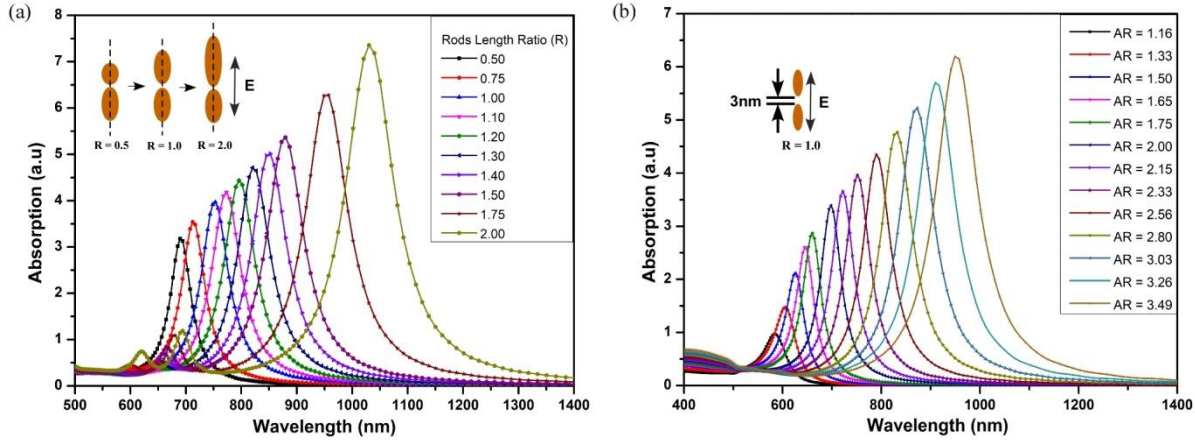


Figure 4. (a) Absorption spectra with increasing R , *i.e.*, increasing the length of one rod and keeping the other rod dimension constant. (b) Variation of LSPR with an increasing aspect ratio of both rods keeping $R = 1$.

It is interesting to study the plasmon coupling in the dimers with different dimensions arranged in an end-to-end configuration. This is important due to the fact that size heterogeneity exists when the dimers are prepared in the laboratory and of great concern. Our investigation is focused on the size mismatch impact through the FDTD simulation, and the results are shown in Figure 4 (a). We observed the sensitivity of the antibonding mode due to its heterogeneity in size. The geometry of the dimers is described by the ratio, R , which is the ratio of the aspect ratio of the nanorods in the dimer. It has been found that the aspect ratio of the nanorod is an important parameter of the longitudinal plasmon energy since the LSPR is approximately a linear function of it. In our simulations, gold nanorods having the same diameter but different lengths have been considered. To change the ratio, R , the length of the bottom nanorod was kept fixed while the length of the top nanorod was altered. A close look at the spectral distribution (between

640 and 700 nm) in Figure 4 (a) shows very weak bumps originating from the longitudinal anti-bonding mode. The spectrum displays only a single peak corresponding to the bonding mode for R up to 1.1. The antibonding dimer mode became prominent for heterodimers with $R=1.2$ and placed on the blue side of the bonding mode. As the R -value increases ($R \geq 1.2$), the bonding mode redshifts, and the antibonding mode starts to emerge, and redshifts with higher intensity. A significant absorption peak [see Figure 4(b)], which arises due to the plasmon modes of longitudinal bonding, is observed above 700 nm for all the homo-dimers ($R = 1$). For dimers with $R \neq 1$, the mirror geometry is no more holds good, leading to a non-zero dipole moment for the antibonding modes, and as a result, a weak peak is observed on the higher energy side of the absorption spectrum. In any dimer, if the absorption cross-section of one nanoparticle is slightly greater than that of the neighboring nanoparticle, then the absorption properties would be dominated by the larger nanoparticle irrespective of which nanoparticle gets excited first.²⁶ The coupled plasmon resonance is red-shifted compared to the plasmon resonance of individual nanorods. This finding shows that even if the distance between the nanorods is kept constant, the coupled plasmon energy of the dimer can be regulated desirably by adjusting the size of the individual metal nanorods. It has been understood that the plasmonic interactions highly dependent on the configuration of nanorods in the dimer. When excited by polarized light along the length of the nanorods in end-to-end homo-dimers, it is red-shifted coupled plasmon mode whereas, for side-by-side homo-dimers, it is significantly blue-shifted. For the linear, end-to-end structure, the coupled plasmon mode has a bonding nature, and it has an anti-bonding character for the side-by-side configuration.

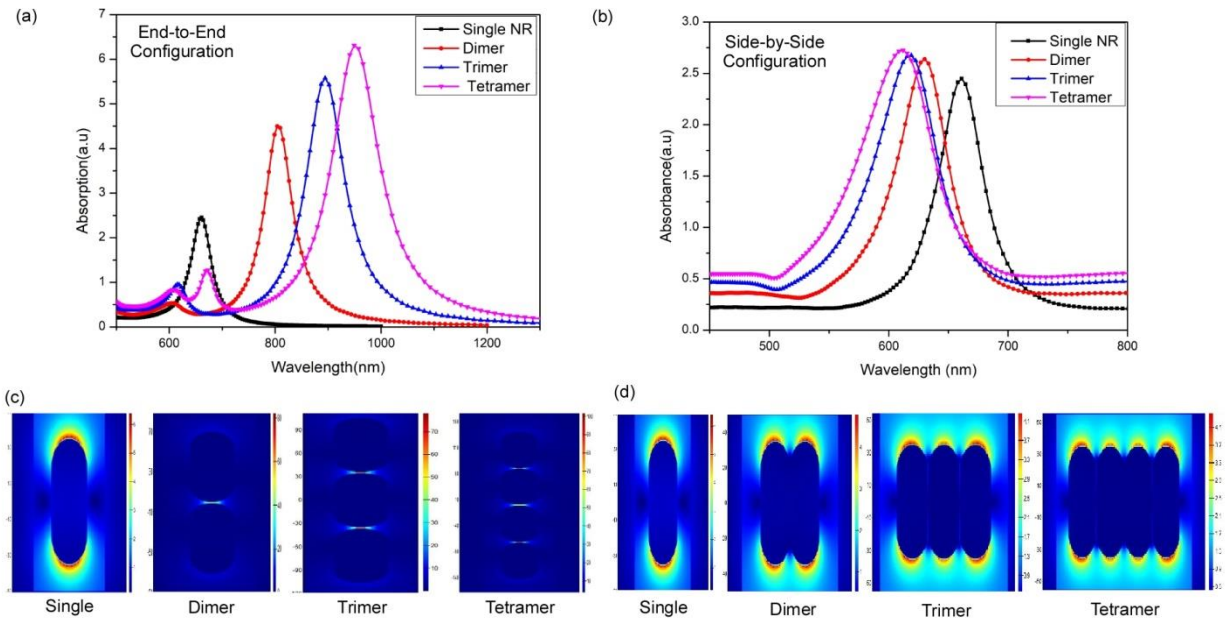


Figure 5. Absorption spectrum of different nanostructure geometry of aspect ratio 2.33 with (a) end-to-end (b) side-by-side configurations. Electric field mapping of the orientation in (c) end-to-end (d) side-by-side configurations.

Now a comparative analysis of single NR, dimer, trimer and tetramer orientation of identical nanorods of aspect ratio 2.33 has been done to understand a larger structure with more number of NRs. We analyzed the side-by-side and end-to-end configuration structures. The gold nanorods are positioned end-to-end in various forms with a separation of 1 nm. The single nanorod shows longitudinal plasmon resonance around ~ 660 nm [Figure 5(a)]. About ~ 605 nm and ~ 805 nm, two plasmon peaks are provided by the dimer configuration corresponding to the anti-bonding and bonding modes, respectively. Likewise, the trimer shape also gives two extremes around ~ 615 nm and ~ 895 nm, and there are peaks at 608 nm, 672 nm, and 950 nm in the tetramer form. The second peak around 672 nm is due to more hot spots created by the assembly structures. As a result, more particles forming the same configuration in a single chain

will also strengthen the plasmon resonance to a higher wavelength. We can see that the plasmon resonance increases from 660 nm to 950 nm as the arrangement differs from single particle to tetramer type. When GNRs are adjacent to each other, the electric field enhancement is often significant; this enables the local field to be coupled and contributes to higher field values in the area between the GNRs. In the dimer configuration, as shown in Figure 5(c), the electric field increased compared to the single nanorod with a maximum enhancement factor of 6. In the chain, due to the electric field, the electric charge oscillates, and the maximum field intensity is always distributed in the gap zone. Hence, as NRs get closer to each other, the opposite charges distribute alternatively, leading to increased interactions. It has been found that the electric field is enhanced many folds in a specific point, which is called hot spots as compared to the rest of the system.

The absorption spectra of the gold nanorods (with AR= 2.33), configured in a side-by-side orientation with a separation of 1 nm, are shown in Figure 5 (b). The dimer configuration gives a 630 nm plasmon peak, whereas the side-by-side trimer of GNRs shows plasmon resonance around ~ 615 nm, while the tetramer of GNRs shows a peak around ~ 612 nm. These side-by-side assembly configurations are blue-shifted in the plasmon resonance from 660 nm to 612 nm. When GNRs are closer in a side-by-side ensemble, the electric field enhancement is weaker, as shown in Figure 5 (d). In the higher configuration, we observe the diminished electric field related to the single nanorod and equivalent for all higher configurations. Therefore, the electric field enhancement is not influenced by this side-by-side assembly configuration. The highest field strength is at the edge surface of the nanorod in the side-by-side assembly.

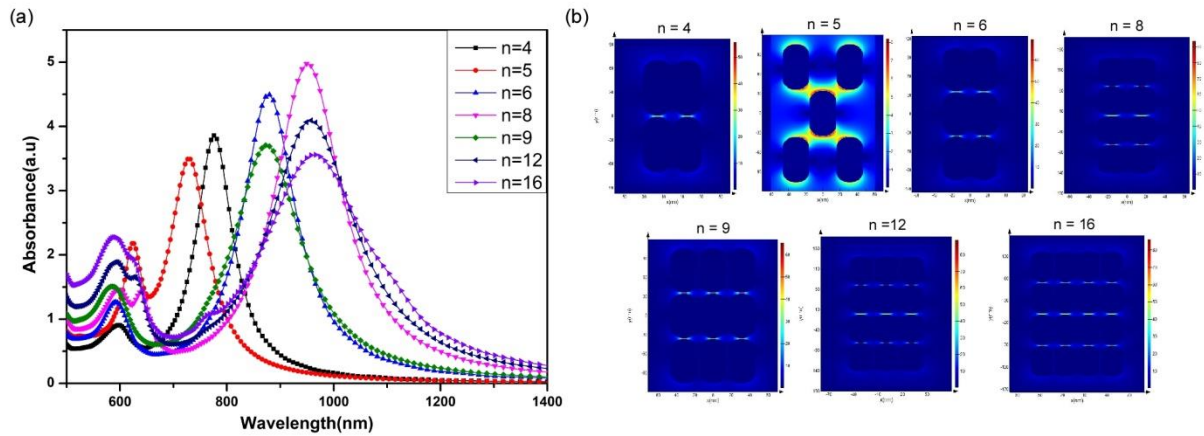


Figure 6. (a) Absorption spectra and (b) electric field distribution mapping of different nanostructures with 'n' number of gold nanorod in various arrays.

We investigated the strength of coupling between the longitudinal plasmon resonances in various end-to-end directed structures containing gold nanorods ($n = 4 - 16$). We observed the overall influence of the various nanostructures on the plasmon coupling and compared it with the dimer, trimer, and tetramer assembly structure. The spacing between the nanorods has been kept at 1 nm so that the near-fields of the individual nanorods interact strongly. We display the respective absorption spectra for different structures in Figure 6 (a) and their electric field distribution in Figure 6 (b). As shown in Figure 6 (a), the LSPR redshifts with an increasing number of nanorods with the same orientation type, as it varies from other structures like 5 NRs. Therefore, plasmon coupling relies on the orientation of the particle for the same size and shape. We observed that increasing the number of particles increases the optical strength, reducing their multiple nanorods structure. The multiple side-by-side trimer structure with the same orientation type, i.e. (3, 6, 9) with an odd number of nanorods, indicates that the peak value is in the same range with a variation of ± 4 nm, and the peak intensity decreases when the structure becomes larger. Similarly, with the same type of orientation, i.e. (4, 8, 12, 16) with an even number of

nanorods, the multiples of the side-by-side tetramer structure indicate that the peak value is in the same range with a variation of ± 5 nm, while the peak intensity decreases when the system becomes larger. Therefore, the large cluster of nanorods can be related to their first chain of nanorods of the same direction as they exhibit almost similar optical absorption and electric field enhancement.

The optical properties of a 4×4 periodic matrix structure of gold nanorods separated by a distance of 1 to 70 nm have been investigated, and the results are shown in Figure 7. We found that the absorption cross-section does not exhibit resonances with consistent symmetrical line profiles. We tried to understand the properties based on particle spacing, which correlates with the electric field enhancements. We increased the separation among the nanorods from 1 to 70 nm to understand the coupling between the light and resonance modes leading to Fano-like resonance. In turn, the array of nanorods exhibits some hybrid modes arising from plasmon resonances of the various nanorods. The hybrid modes resonate as bonding mode at a higher wavelength and as an anti-bonding mode at a lower wavelength with an FWHM much broader for the bonding mode than the anti-bonding mode [see Figure 7 (a)]. The bonding mode blue-shifted exponentially from 965 nm to 670 nm [Figure 7 (b)] and the anti-bonding mode red-shifted from 585 nm to 650 nm with increasing resonance peak intensity. The electric field enhancement of the system also decreases exponentially by increasing the gap from 1 to 70 nm, as shown in Figure 7 (b). We can see from Figure 7 (c) that the interaction between the rods decreases with increasing separation distance, and the individual features become prominent with no significant interaction among the individual rods.

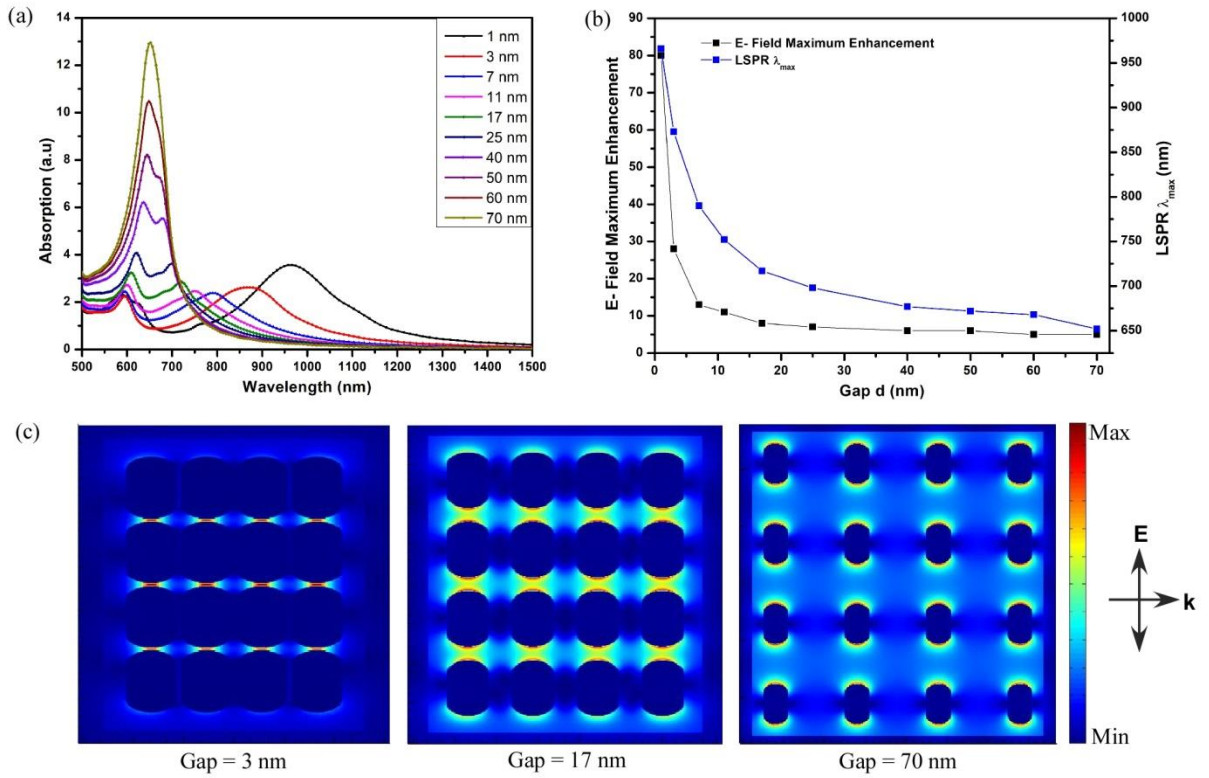


Figure 7. (a) Absorption spectra of 4×4 array structure with the variation of the gap, (b) variation of LSPR and electric field enhancement with the separation of the gap, d in nanoparticles, and (c) electric field mapping at different separation gap *namely* 3 nm, 17 nm, and 70 nm.

The resonant modes' spectral overlap can explain the fano-like resonance, and the asymmetry primarily arises from the bonding coupling phase of the above array structure. The configurations size of nanorods in structure and the conditions of illumination influence both the absorption and coupling of individual resonant modes. This is well reflected in the total optical properties of the array structures.⁴⁰ The Fano dip of the absorption spectrum slowly disappears as the distance between the nanorods increases, and the spectrum transforms into a single Lorentzian resonance band. The electric field enhancement contributions often indicate a shift from asymmetric to symmetric line profiles as the separation increases in the structure. The

result suggests that a minimum gap size is needed to achieve a Fano-type resonance. It is possible to view the variation in the resonance line profiles with increasing the gap between the nanorods. In the separation gap of ≥ 60 nm, the coupling between these nanorods is no longer strong enough to distinguish both modes and exhibit a Lorentzian characteristic of an independent nanorod. The increase in the separation distance among nanorods results in blue shifts followed by exponential decay behavior, shortening the fano dip in the absorption spectra. The contribution of various modes to the absorption spectra indicates an increase in the relative intensity of the peak with a decrease in the electric field by increasing the separation distance. These behaviors illustrate the importance of separation between nanorods in array size to optical efficiency, which is critical in structure design for relevant applications.

4. Conclusion

The plasmon coupling between gold nanorods depends on their relative orientation and interparticle spacing. A detailed understanding of plasmon coupling in gold nanorod dimers in different geometry has been studied using the FDTD simulation methodology. We discussed the response by varying the size heterogeneity and rotational geometries. Plasmon hybridization corresponds to anti-bonding, and bonding modes have been observed in our studies. The plasmon coupling has also been studied by varying the aspect ratio of one nanorod and keeping another nanorod constant with a small spacing between the nanorods. The increase in spacing leads to a decrease in the electric field enhancement. In a heterodimer, anti-bonding dimer modes that would not be noticeable compared to the homodimers emerge clearly in the spectrum. The angular-related coupling shows that the electric field enhancement happens only when the bonding plasmon mode is excited by external light. The large nanorod ensembles may be compared to their small ensemble structure of the same orientation, as the optical absorption and

electric field enhancement are precisely in the same region. This plasmonic coupling of different sizes (monomers, dimers, trimers, tetramers) of nanorods presents a better tool for tuning the frequency, intensity, spatial distribution, and polarization of local electric field inside and around nanostructures. There is an interaction between broad and narrow resonant modes in a 4×4 array structure of gold nanorods, resulting in a Fano resonance with its distinctively asymmetric line shape. The signature Fano dip of the extinction spectrum gradually disappears as increasing the distance between the nanorods and turns into a single Lorentzian-shaped resonance band. We observed that plasmon coupling depends on four factors, namely, the distance of separation, orientation, size heterogeneity, and the number of nanorods in the geometry. Understanding the dependence on the number, distance, and orientation between the nanorods of collective plasmonic properties provides a functional layout for developing different applications.

AUTHOR INFORMATION

Corresponding Author

**Aditya K. Sahu - Department of Physical Sciences, Indian Institute of Science Education and Research Kolkata, Mohanpur, Nadia 741246, India*

Email: aks16rs023@iiserkol.ac.in

Authors

Aditya K. Sahu - Department of Physical Sciences, Indian Institute of Science Education and Research Kolkata, Mohanpur, Nadia 741246, India

Satyabrata Raj - *Department of Physical Sciences, Indian Institute of Science Education and Research Kolkata, Mohanpur, Nadia 741246, India*

ORCID iDs

Aditya K. Sahu: 0000-0003-2405-5906

Satyabrata Raj: 0000-0003-2193-3152

Acknowledgments

The author, AKS acknowledges CSIR, Government of India for financial support.

Author Contribution

All authors contributed to the study conception and design. Simulation, Software, data collection and analysis were performed by [Aditya K. Sahu]. The manuscript was written by both authors. Both authors read and approved the final manuscript.

Notes

The authors declare no competing financial interest.

References

1. Nie S and Emory S R 1997 *Science* **275** 1102-06.
2. Wang X, Yao L, Chen X, Dai H, Wang M, Zhang L, Ni Y, Xiao L and Han J 2019 *ACS Appl. Mater. Interfaces* **11 (35)** 32469-74.
3. Krivenkov V, Goncharov S, Samokhvalov P, Sanchez-Iglesias A, Grzelczak M, Nabiew I and Rakovich Y 2019 *J. Phys. Chem. Lett.* **10** 481–6.

4. Bao Y J, Yu Y, Xu H F, Lin Q L, Wang Y, Li J T, Zhou Z K and Wang X 2018 *Adv. Funct. Mater.* **28** 1805306.
5. Yao L H, Zhang J P, Dai H W, Wang M S, Zhang L M, Wang X and Han J B 2018 *Nanoscale* **10** 12695–703.
6. Dai H, Zhang L, Wang Z, Wang X, Zhang J, Gong H, Han J. B and Han Y 2017 *J. Phys. Chem. C* **121** 12358–64.
7. Ma Z W, Chi C, Yu Y, Zhong Z Q, Yao L H, Zhou Z K, Wang X, Han Y B, and Han J B 2016 *Opt. Express* **24** 5387–94.
8. Zhou Z K, Liu J, Bao Y J, Wu L, Png C E, Wang X H, Qiu C W 2019 *Applied. Prog. Quantum Electron* **65** 1–20.
9. Zhang L M, Dai H W, Wang X, Yao L H, Ma Z W, Han J B 2017 *J. Phys. D: Appl. Phys.* **50** 355302.
10. Li J, Cushing S K, Meng F, Senty T R, Bristow A D, and Wu N 2015 *Nat. Photonics* **9** 601–8.
11. Sheldon M T, van de Groep J, Brown A M, Polman A, and Atwater H A 2014 *Science* **346** 828–31.
12. Kreibig U, Vollmer M *Optical Properties of Metal Clusters*; Springer: Berlin, 1995.
13. Kelly K L, Coronado E, Zhao L L, and Schatz G C 2003 *J. Phys. Chem. B* **107** 668–77.
14. Sheikholeslami S, Jun Y W, Jain P K, and Alivisatos A P 2010 *Nano Letters* **10** (7) 2655-60.
15. Shao L, Ruan Q F, Jiang R B, and Wang J F 2014 *Small* **10** 802–11.
16. Lee J, Tymchenko M, Argyropoulos C, Chen P Y, Lu F, Demmerle F, Boehm G, Amann M C, Alu A, and Belkin M A 2014 *Nature* **511** 65–69.

17. Shao L, Woo K C, Chen H J, Jin Z, Wang J F, and Lin H Q 2010 *ACS Nano* **4** 3053–62.
18. deWaele R, Koenderink A F, and Polman A 2007 *Nano Lett.* **7** 2004–8.
19. Zuloaga J, Prodan E, and Nordlander P 2009 *Nano Lett.* **9** 887–91.
20. Slaughter L S, Wu Y, Willingham B A, Nordlander P, and Link S 2010 *ACS Nano* **4** (8) 4657-66.
21. Prodan E, Radloff C, Halas N J, and Nordlander P A 2003 *Science* **302** 419–22.
22. Yoon J H, Selbach F, Schumacher L, Jose J, and Schlücker S 2019 *ACS Photonics* **6** (3) 642-8.
23. Li W Y, Camargo P H C, Lu X M, and Xia Y N 2009 *Nano Lett.* **9** 485–90.
24. Kim S, Jin J, Kim Y J, Park I Y, Kim Y, and Kim S W 2008 *Nature* **453** 757–60.
25. Kinkhabwala A, Yu Z F, Fan S H, Avlasevich Y, Mullen K, and Moerner W E 2009 *Nat. Photonics* **3** 654–7.
26. Ueno K, Juodkazis S, Mizeikis V, Sasaki K, and Misawa H 2008 *Adv. Mater.* **20** 26–30.
27. Grigorenko A N, Roberts N W, Dickinson M R, and Zhang Y 2008 *Nat. Photonics* **2** 365–70.
28. Muhlschlegel P, Eisler H J, Martin O J F, Hecht B, and Pohl D W 2005 *Science* **308** 1607–9.
29. Schnell M, Garcia-Etxarri A, Huber A J, Crozier K, Aizpurua J, and Hillenbrand R 2009 *Nat. Photonics* **3** 287–91.
30. Jain P K, Eustis S, and El-Sayed M A 2006 *J. Phys. Chem. B* **110** 18243–53.
31. Lisunova M, Norman J, Blake P, Forcherio G T, DeJarnette D F and Roper D K 2013 *J. Phys. D: Appl. Phys.* **46** 485103.

32. Shcherbakov M R, Vabishchevich P P, Komarova V V, Dolgova T V, Panov V I, Moshchalkov V V and Fedyanin A A 2012 *Phys. Rev. Lett.* **108** 253903.
33. Zou S and Schatz G C 2005 *Chem. Phys. Lett.* **403** 62.
34. Samson Z L, Macdonald K F, Angelis F D, Cholipour B, Knight K, Huang C C, Fabrizio E D, Hewak D W and Zheludev N I 2010 *Appl. Phys. Lett.* **96** 143105.
35. Lumerical Solutions, Inc. (trial version),
www.docs.lumerical.com/en/fdtd/reference_guide.html
36. Johnson P B, and Christy R W 1972 *Phys. Rev. B* **6** 4370 - 9.
37. Tabor C, Haute D V, and El-Sayed M A 2009 *ACS Nano* **3 (11)** 3670-8.
38. Wu J, Lu X, Zhu Q, Zhao J, Shen Q, Zhan L, and Ni W 2014 *Nano-Micro Lett.* **6(4)** 372–80.
39. Biswas S, Nepal D, Park K, and Vaia R A 2012 *J. Phys. Chem. Lett.* **3** 2568–74.
40. Bakhti S, Tishchenko A V, Zambrana-Puyalto X, Bonod N, Dhuey S D, Schuck P J, Cabrini S, Alayoglu S and Destouches N 2016 *Sci. Rep.* **6** 32061.